High resolution dynamic mapping of the *C. elegans* intestinal brush border

Aurélien Bidaud-Meynard[1], Flora Demouchy[1,2], Ophélie Nicolle[1,2], Anne Pacquelet[1,2] and Grégoire Michaux[1,*]

[1]Univ Rennes, CNRS, IGDR (Institut de Génétique et Développement de Rennes) - UMR 6290, F-35000 Rennes, France

[2]These authors contributed equally to this work

[*]lead contact gmichaux@univ-rennes1.fr

Abstract

The intestinal brush border is made of an array of microvilli that increases the membrane surface area for nutrient processing, absorption, and host defence. Studies on mammalian cultured epithelial cells uncovered some of the molecular players, structural components and physical constrains required to establish this apical specialized membrane. However, the building and maintenance of a brush border *in vivo* has not been investigated in detail yet. Here, we combined super-resolution imaging, transmission electron microscopy and genome editing in the developing nematode *C. elegans* to build a high-resolution and dynamic localization map of known and new markers of the brush border. Notably, we show that microvilli components are dynamically enriched at the apical membrane during microvilli outgrowth and maturation but become highly stable when microvilli are built. This new mapping tool will be instrumental to understand the molecular processes of microvilli growth and maintenance *in vivo* as well as the effect of genetic perturbations, notably in the context of disorders affecting the brush border integrity.

Introduction

The tremendous intestinal exchange surface required for efficient nutrient absorption is reached through three consecutive morphogenic processes in mammals: elongation of the intestinal tube, generation of villus protrusions and establishment of microvilli at the surface of each enterocyte, which together amplify the tube area nearly 100-times (Walton et al., 2016). Generation of microvilli in mammals occurs during enterocyte differentiation along the crypt-villus axis with the nucleation of actin filaments anchored on an F-actin- and intermediate filament-based terminal web. These core-actin bundles are then organized into a well-ordered and tightly packed array by various actin crosslinking and bundling factors, among which villin, espin and plastin1/fimbrin play a major role (Sauvanet et al., 2015). Recent studies in epithelial cell lines identified new functional players, such as IRTKS or myosin 1a/6/7b (Crawley et al., 2014a, Postema et al., 2018), and new mechanisms of brush border assembly and maintenance by intracellular trafficking (Vogel et al., 2015), microvilli motility, contraction and clustering (Meenderink et al., 2019, Chinowsky et al., 2020) or intermicrovillar protocadherin bridges (Crawley et al., 2014b). Additionally, recent use of live imaging revealed some of the key initiation and maturation steps of microvilli biogenesis in cell lines (Gaeta et al., 2021).

The intestine of the soil nematode *C. elegans* has been widely used as a *in vivo* model of intestinal luminogenesis, polarity, and host defence (Zhang et al., 2013, Zhang and Hou, 2013, Sato et al., 2014, Shafaq-Zadah et al., 2012). The *C. elegans* intestine is composed of perennial intestinal epithelial cells, contrary to the ~3-5-days living mammalian enterocytes that arise from the proliferation of crypt based columnar stem cells (Walton et al., 2016, McGhee, 2007). Intestinal organogenesis in *C. elegans* encompasses cell division and intercalation steps from the E blastomere ancestor to form a primordium containing two rows of eight cells (E16 stage) which ends up, after a last round of division, with twenty cells arranged into nine rings (or *ints*) forming a ellipse-shaped tube that runs along the whole body

of the worm (Leung et al., 1999, Asan et al., 2016). Polarization of the intestinal cells begins at the two-tiered E16 stage with the enterocyte polarization, giving rise to a basolateral and an apical pole, later covered by microvilli, separated by the CeAJ junctional complex. Polarization, which encompasses cellular components relocalization and cell shape changes (Leung et al., 1999), relies on the recruitment of the polarity determinant PAR-3 at the apical membrane which recruits the other members of the apical PAR polarity complex (Achilleos et al., 2010) and plays a major role in intestinal function (Feldman and Priess, 2012, Sallee et al., 2021). Luminogenesis also occurs at the E16 stage with the formation of apical cavities at the midline that ultimately form a lumen, a process that probably involves vesicular trafficking (Leung et al., 1999). Despite the absence of villar protrusions, the apical aspect of *C. elegans* enterocytes displays a brush border that is structurally similar to that of mammals (Leung et al., 1999, Geisler et al., 2019, Bidaud-Meynard et al., 2019) and relies on some of the same structural components. Indeed, *C. elegans* microvilli are made of F-actin core bundles, notably the intestinal-specific isoform of actin *act-5*, whose depletion induces a circular lumen with sparse and defective microvilli (MacQueen et al., 2005). Several F-actin regulators have been shown to be essential for *C. elegans* microvilli integrity, such as *erm-1* (the ortholog of the member of the Ezrin/Radixin/Moesin family of F-actin plasma membrane crosslinkers ezrin) (Gobel et al., 2004, Van Furden et al., 2004) and the actin capping factor EPS-8 (Croce et al., 2004). As in mammals, these microvilli are anchored on a terminal web made of a network of F-actin and various intermediate filament isoforms (Bossinger et al., 2004), the latter forming an electron-dense belt named as endotube, in which IFB-2 seems to play a major role (Geisler et al., 2020). Hence, the structural and biochemical similarity with mammals make *C. elegans* an appropriate model to study the biogenesis of microvilli *in vivo*.

In that context, most of the studies in *C. elegans* focused on the polarized localization of markers and the fate of the brush border was only studied by Transmission Electron

78 Microscopy (TEM), which provides ultrastructural data but lacks the dynamics and whole organ
79 context. Very recently, some studies, including our, started to use *in vivo* super-resolution
80 microscopy to study the apical membrane of *C. elegans* intestinal cells (Bidaud-Meynard et al.,
81 2019) and excretory canal (Khan et al., 2019). Here, we combined optimized super-resolution
82 and quantitative live microscopy, TEM and fluorescence recovery after photobleaching to study
83 the recruitment and dynamics of endogenously tagged markers during the establishment of the
84 brush border *in vivo* in *C. elegans*.
85

Results and discussion

TEM analysis of the brush border establishment in *C. elegans* developing embryo.

To first characterize the development of the brush border *in vivo*, embryos and larvae at various developmental stages were analysed by TEM using an optimized method (Nicolle et al., 2015, Kolotuev et al., 2009). We observed that the intestinal lumen starts to open at the Comma stage and progressively expands to reach the renown elliptic shape in larvae (Fig. 1A-B). At the apical PM, the first microvilli-like membrane extensions were observed at the 1.5-fold stage and started to cover the apical pole, with a disorganized pattern, at the 2,5-fold stage, and finally formed a regular brush border from the 3-fold stage (Fig. 1A). Measurement of microvilli density, length and width allowed to determine two phases of brush border biogenesis: 1) an *initial assembly* phase (1.5-fold to 4-fold stage), where ~72% of the total microvilli are assembled *de novo* (Fig. 1C), and 2) a *maturation* phase (4-fold to adulthood), where assembled microvilli grow in length and width, in a stepwise and continuous manner, respectively (Figs 1A-E and S1A-C). This latter process also encompasses the growth of some microvilli to fill the virtual empty spaces left by intestinal surface expansion to reach the final brush border density (Fig. 1A, 4-fold). Finally, the brush border could be imaged transversally in adult worms (Fig. 1F), which allowed to measure the distance between microvilli edges and centres (76,0 ± 1,1 nm and 203,2 ± 2,0 nm, respectively) (Fig. 1G).

Dynamic recruitment of brush border components during *C. elegans* development.

Expression profiling in mammalian enterocytes between the proliferative crypt and the terminally differentiated villus demonstrated a marked upregulation of actin-related cytoskeletal genes, including actin, ezrin, villin and espin (Chang et al., 2008, Mariadason et al., 2005). Notably, recent data in LLC-PK1 cells showed a stepwise recruitment of EPS8 and IRTKS before (initiation) and ezrin during (elongation) microvilli growth (Gaeta et al., 2021). We hypothesized that a set of brush border components may specifically be recruited at the

apical pole during brush border establishment *in vivo*. To test this, we performed a systematic analysis of the apical localization of endogenously tagged known brush border markers and putative new components, based on expression patterns as well as sequence or function homology with human proteins.

First, this led to the identification of two new structural components of *C. elegans* enterocytes apical membrane: i) PLST-1, the ortholog of plastin1/fimbrin (Figs 2A and S2), which is one of the major F-actin organizing factor in mammalian cells brush borders (Crawley et al., 2014a), together with ezrin, villin and espin. While the ortholog of villin seems not to be localized at the brush border (Hunt-Newbury et al., 2007) and espin does not have a *C. elegans* ortholog, PLST-1 has been involved in cortical contractility in *C. elegans* zygote (Ding et al., 2017) but has not been studied in the intestine yet; ii) FLN-2 (the ortholog of filamin A) (Figs 2B and S2), a F-actin cross-linker that has been proposed to play a role in brush border maintenance in mammalian models but not in *C. elegans* (Zhou et al., 2014).

Second, most of the myosin classes have been localized to the brush border in mammalian cells where they play both a structural (e.g. MYO7b, MYH14) and trafficking (e.g. MYO-1a, -6) role (Chen et al., 2001, Heintzelman et al., 1994, Sauvanet et al., 2015, Houdusse and Titus, 2021). We found that a specific set of myosins accumulates at the enterocytes apex throughout *C. elegans* development: i) the unconventional heavy chain HUM-5 (the ortholog of human MYO1d/g) which is also localized at the lateral membrane, but not the other members of this class, HUM-1 and HUM-2 (Figs 2C, S2 and S3A-B); ii) the essential myosin light chain MLC-5 (Gally et al., 2009) (the ortholog of human MYL1/6) accumulated at the apical membrane of the enterocytes in both embryos and larvae, while MLC-4 was only weakly expressed in embryos (Figs 2D, S2 and S3C). Interestingly, we found that the non-muscle heavy chain myosins NMY-1 and NMY-2 (the orthologs of MYH9/10 and MYH10/14, respectively) (Fig. S3D-E), did not, or only very weakly for NMY-1, accumulate at the apical pole, which

suggests that myosin-dependent contractility may be less crucial for microvilli assembly in *C. elegans* than in mammals (Chinowsky et al., 2020). Furthermore, we have not investigated the presence of intermicrovillar bridges molecules, such as protocadherin complexes (Crawley et al., 2014b), despite a putative hexagonal arrangement of microvilli (Figs 1F and 3D). These results suggest species-specific mechanisms or compensation between myosins, as shown before (Houdusse and Titus, 2021), and the need for systematic approaches to better characterize the conserved components of brush borders.

To quantitatively assess the expression of these apically enriched factors during brush border establishment, we used photon counting detectors and quantified the absolute apical signal of endogenously tagged proteins at all *C. elegans* developmental stages (Fig. 2K, S2, S3F). Notably, we observed that a set of markers was already localized at the apical PM at the lima bean stage, before microvilli onset as observe by TEM: ERM-1, FLN-2, PLST-1, ACT-5 (note that ACT-5 was exogenously expressed under its own promoter, because of the embryonic lethality of endogenously tagged strains), and the intermediate filament IFB-2 (Figs 2E-J and S2). Then, we observed that the apical localization of these markers, as well as that of EPS-8, HUM-5 and MLC-5, dramatically increased concomitantly with microvilli assembly (from the 1,5-fold stage), most of them peaked between the 4-fold and L1 stages and then decreased until adulthood (Fig. 2K-S and S2). The early accumulation of the cytoskeletal protein ERM-1 and ACT-5 mirrors their requirement for microvilli assembly (Gobel et al., 2004, MacQueen et al., 2005), and the direct relationship between G-actin apical availability and microvilli growth (Faust et al., 2019). As PLST-1 also accumulated before microvilli onset, it could also play a role in microvilli initial assembly *in vivo*, which is coherent with the disorganized terminal web and microvilli rootlets described in *Pls1* knockout mice (Grimm-Gunter et al., 2009). Its relative but specific disappearance only at the comma stage might suggest that this stage corresponds to a specific time just before the formation of the first microvilli. Interestingly, we observed

that FLN-2 displayed a shifted pattern, with an earlier apical accumulation that may suggest a specific role in microvilli establishment that needs to be analysed in detail. Thus, as in mammalian cells (Gaeta et al., 2021), *C. elegans* microvilli assembly might rely on an *initiation complex*, composed, at least, of ERM-1, ACT-5, PLST-1, FLN-2 and IFB-2, and an *elongation/maturation complex*, composed additionally of the actin polymerization/severing agent EPS-8, HUM-5 and MLC-5 (Fig. S5B).

Super-resolution imaging of the brush border *in vivo*

To visualize the precise localization of brush border markers, we first developed an imaging set up that would allow to resolve individual microvilli (~100 nm interspaced, ~120 nm wide, Fig. 1E, G). According to the Rayleigh criterion ($Rfluo = \frac{1.22\lambda}{2xNA}$), the optical axial resolution of the 405, 488 and 561 nm lasers is theoretically of 176.5, 212.6 and 244.4 nm, respectively. To test this theoretical resolution *in vivo*, we inserted by CRISPR-CAS9 three different tags at the C-terminal end of the brush border-specific factor ERM-1: Blue Fluorescent Protein (mTagBFP2/BFP, λ_{Ex} 381 nm/λ_{Em} 445 nm), mNeongreen (mNG, λ_{Ex} 506 nm/λ_{Em} 517 nm) (Shaner et al., 2013) and wrmScarlet (wSc, λ_{Ex} 569 nm/λ_{Em} 593 nm) (El Mouridi et al., 2017) and imaged them with a multi-detector and deconvolution-based super-resolution imaging system (see methods). We could easily visualize the regular alignment of microvilli with BFP and mNG tags, but it was less visible with the wSc fluorophore (Fig. 3A-B). In addition to individual microvilli, we could also precisely localize brush border markers along the microvilli long axis. Indeed, while ERM-1 covered the whole microvilli length, the chloride intracellular channel 2 (CLIC-2) ortholog EXL-1 (Liang et al., 2017) and the P-GlycoProtein related transporter PGP-1 (Broeks et al., 1995), accumulated at the tip and the base of the microvilli, respectively (Fig. 3C) (Bidaud-Meynard et al., 2019). Of note, this method allowed to uncover small localization differences between in locus mNG-tagged and overexpressed GFP-tagged proteins (compare Figs 3C and S4A). Individual microvilli were similarly

visualized using Random Illumination Microscopy (Mangeat et al., 2021), but not using conventional confocal imaging or Stimulated-emission-depletion (STED) microscopes, probably because of the depth of the intestine inside the nematode body (~15µm) (Figs 3C and S4B). The brush border could also be imaged transversally (compare Fig. 3D and 1F). Hence, the combination of a specific super-resolution imaging system and appropriate fluorophores allows the precise visualization of microvilli *in vivo* in *C. elegans* intestine.

We then used this new tool to study the (co)localization of known and newly identified apical markers in adult worms, as we have done before for ERM-1 and ACT-5 (Bidaud-Meynard et al., 2019). Using a strain co-expressing endogenously tagged versions of the three classical microvilli markers ERM-1, EPS-8 and IFB-2, we observed that ERM-1 localized along the whole microvilli but not in the terminal web (Fig. 3E). EPS-8 accumulated at the tip of the microvilli, where it partially colocalized with ERM-1, and was also found marginally at the terminal web vicinity, as observed before by immuno-EM (Croce et al., 2004) (Fig. 3E). Finally, we could resolve in some worms the tiny difference between ACT-5, which localized along and at the basis of the microvilli, and the endotube marker IFB-2 (Geisler et al., 2019, Bossinger et al., 2004), with which it composes the terminal web (Fig. S4C).

Notably, we found that PLST-1 localized at the bottom of the microvilli (Fig. 3F), with a doted pattern different from the linear terminal web pattern (Figs 3E). This localization is consistent with that of Plastin-1 in mouse jejunum sections and its proposed role in anchoring microvillar actin rootlets to the terminal web (Grimm-Gunter et al., 2009). While FLN-2 was hardly detectable in adult worms, we observed in L1 larvae that FLN-2 localized at the basis of microvilli (Fig. 3G), alike MLC-5 (Fig. 3H). Finally, we found that HUM-5 localized both at the basis and the tip of microvilli (Fig. 3I), a similar pattern to that described in mouse intestine (Benesh et al., 2010). Thus, our novel methodology allowed to visualize *in vivo* the expression

and the precise localization of several proteins of the brush border including structural and trafficking factors as well as molecular motors.

Since factors needed to build the microvilli are concomitantly recruited to the apical pole (Fig. 2), we finally asked whether super-resolution imaging could resolve the change in their relative microvillar position during brush border assembly. Line scans showed that ERM-1, EPS-8 and IFB-2 colocalized at the beginning of microvilli assembly (2-fold stage) and progressively moved away to end up with IFB-2 and EPS-8 contralaterally positioned and surrounding ERM-1 (Figs 3J-K and S4D).

Analysis of brush border markers dynamics during microvilli assembly

The progressive accumulation of brush border components at the apical PM implies a dynamic behaviour during microvilli building (Fig. 2K), consistent with the intense actin treadmilling (half-time recovery of ezrin of ~30 s) in immature microvilli from non-polarized cells models (Garbett and Bretscher, 2012). However, their decreased apical expression after the L1 larval stage may reflect a high stability of mature brush borders, as also proposed recently *in vivo* in adult worms (Ramalho et al., 2020, Remmelzwaal et al., 2021), and which would explain their uniform length and highly ordered organisation in the human intestine (Crawley et al., 2014a). To test this conjecture, we analysed the dynamics of ERM-1 during and after the establishment of the brush border using *fluorescence recovery after photobleaching* (FRAP) experiments. While ERM-1 was very dynamic during microvilli assembly (1,5-fold embryo) it became surprisingly very stable in established brush border (adult worm), with little recovery even after >15 minutes (Figs 4A and S5A). Systematic analysis of ERM-1 fluorescence recovery throughout *C. elegans* development confirmed that ERM-1 dynamics progressively decreased concomitantly with brush border assembly and became almost static in larvae and adults (Fig. 4B, F). To confirm this, the dynamics of other structural components of the brush border was analysed during microvilli initial assembly (Comma/1,5-

fold), maturation (L1 larvae) and in adult worms; note that due to embryo fast movements from the 2-fold stage to the end of embryogenesis, these developmental stages could not be investigated. Like ERM-1, EPS-8 was also very dynamic during microvilli assembly but became very stable in maturating and mature microvilli (Fig. 4C, F). ACT-5 also displayed a dynamic, albeit of a lower extend, behaviour, that persisted until L1 larvae (Fig. 3D, F), which is in the range of microvillar actin mobile fractions in Caco-2 cells (~60%) (Waharte et al., 2005), to finally become stable at adulthood. Conversely, the intermediate filament IFB-2 displayed a more stable behaviour at every developmental stage, which reflects its anchoring role for growing microvilli (Grimm-Gunter et al., 2009, Geisler et al., 2019).

Thus, these results enlightened that mature microvilli adopt a stable steady state *in vivo,* which is consistent with the notion that microvilli might be considered more as stereocilia than evanescent F-actin-based structures like filopodia. The maturation status of the brush border might be a key consideration that would help to reconcile conflicting data of the literature, where probably immature microvilli in non-polarized cells seem to be more dynamic, i.e. life-cycle of ~12 min in A6 cells (Gorelik et al., 2003) but which were found to last up to 12 h in mature brush borders (Meenderink et al., 2019).

In conclusion, this new multi-imaging approach allowed to image the precise localization of brush border markers at the microvilli level *in vivo* and to study the dynamic recruitment of microvilli components during the development of the brush border. This new methodology will be instrumental to address the many questions remaining to understand microvilli assembly and maturation, notably on the full set of factors required for microvilli growth and maintenance, the principles that govern microvilli size, packing and organization or the motility of microvilli *in vivo*. It will be also instrumental to understand the pathophysiology of diseases affecting the brush border, such as Microvillus inclusions disease

(Bidaud-Meynard et al., 2019), Crohn's (VanDussen et al., 2018) and celiac (Tye-Din and Anderson, 2008) diseases or pathogen infections (Scott et al., 2004, Lauwaet et al., 2004).

Materials and methods

C. elegans strains and maintenance

Strains were maintained under typical conditions as described (Brenner, 1974). CRISPR-CAS9-genome edited mTagBFP2, mNeonGreen and mScarlet-tagged proteins were generated at the « Biologie de *Cænorhabditis elegans* » facility (Universite Lyon 1, UMS3421, Lyon, France). The strains used in this study are listed in Table S1.

in vivo confocal imaging in *C. elegans*

For *in vivo* imaging, *C. elegans* larvae were mounted on a 10% agarose pad in a solution of 100 nm polystyrene microbeads (Polysciences Inc.) to stop worm movement. Embryos were mounted on a 2% agarose pad with a mix of bacteria and M9 medium (localization) or M9 only (live imaging). Single confocal slices of the anterior intestinal cells or stacks were performed on adults/larvae and whole embryos, respectively, using a Leica SP8 (Wetzlar, Germany) equipped with a 63X, 1.4 NA objective (LAS AF software) or a super-resolution Zeiss LSM880-Airyscan (Oberkochen, Germany) equipped with a 63X, 1.4 NA objective (Zen Black software). Quantitative recording of the apical localization of brush border markers was performed on the Leica SP8 microscope using the photon counting function of HyD hybrid detectors and image accumulation process (Fig. S3). For embryos, stacks were reconstructed using the max intensity Z-projection function of Fiji software (https://imagej.net/Fiji). All images were examined using Fiji software. Random Illumination Microscopy was performed at the LITC Core Facility, Centre de Biologie Integrative, Université de Toulouse, France, using the workflow recently published on ERM-1::GFP expressing strains (Mangeat et al., 2021).

TEM

Samples were subjected to high-pressure freezing followed by freeze substitution, flat embedding, targeting, and sectioning using the positional correlation and tight trimming approach, as described previously (Bidaud-Meynard et al., 2019). Each embryo or larva was

sectioned in 5-10 different places, every 5-7 µm, to ensure that different intestinal cells were observed. Ultrathin sections (60-70 nm) were collected on formvar-coated slot grids (FCF2010-CU, EMS) and observed using a JEM-1400 transmission electron microscope (JEOL, Tokyo, Japan) operated at 120 kV, equipped with a Gatan Orius SC 1000 camera (Gatan, Pleasanton, USA) and piloted by the Digital Micrograph program.

Fluorescence recovery after photobleaching (FRAP)

FRAP experiments were performed using the Zeiss LSM880-Airyscan on a rectangle ROI of 120 px width crossing the apical PM with 100% 488 nm laser power, 10-20 iterations and recovery was measured every 30 s for 10 to 15 min. Post-FRAP images were analysed using Fiji software. The mean fluorescence intensity of the bleached ROI was normalized for photobleaching by recording the intensity of the same ROI on a non-bleached region and cytoplasmic background was subtracted on each frame. Finally, the % recovery was calculated on each timeframe by comparing the normalized signal intensities with the mean of two timepoints before bleach. Curve fitting was performed with one-phase association non-linear regression analysis using Graphpad Prism 9 software. The mobile fraction was calculated using EasyFRAP software (https://easyfrap.vmnet.upatras.gr/?AspxAutoDetectCookieSupport=1).

Quantification

Micrographs were analysed using Fiji software and were representative of all the sections observed. Microvilli (length, width, density) and lumen perimeter were quantified on at least 6-13 TEM images per sample (n≥3, by developmental stage).

For the quantitative measurement of the apical localization of brush border markers, a maximum intensity projection was performed using Fiji, and the signal density was quantified by measuring the mean fluorescence signal along a segmented line covering the whole intestine (E16 to 2-fold embryos) or visible part of the anterior intestine (3-fold to adults). The signal

310 measured was then corrected for fluorescence accumulation and normalized for the highest
311 expression level during development.

312 **Statistical analysis**

313 Results are presented as mean ± SEM, as indicated in Figure captions, of the number of
314 independent experiments indicated in the legends, and scattered dots represent individual
315 worms. p-values were calculated by two-tailed unpaired student's t-test or one-way ANOVA,
316 and a 95% confidence level was considered significant. Normal distribution of data and
317 homogeneity of variances were validated using the Shapiro-Wilk and the F-test, respectively.
318 Mann-Withney U-test was used for calculating the P-values of non-normal distributions, and
319 Welch correction was applied to normal distributions with non-homogenous variances.

Acknowledgements

We thank Marc Tramier and Stéphanie Dutertre for their advice on fluorescence quantification and super-resolution imaging, respectively, as well as Matis Soleilhac for the initial analysis of expression patterns. We also thank Michel Labouesse, Junho Lee, François Robin and Ronen Zaidel-Bar for strains as well as Céline Burcklé and Guillaume Halet for helpful discussions. Some strains were provided by the CGC, which is funded by NIH Office of research Infrastructure Programs (P40 OD010440; University of Minnesota, USA). We are grateful to Maité Carre-Pierrat who performed CRISPR-CAS9 endogenous tagging at the Biology of Caenorhabditis elegans Facility, Universite Lyon 1, UMS3421, France. Imaging was performed at the photonic and electron microscopy facilities of the Microscopy Rennes imaging Center (MRiC), member of the national infrastructure France-BioImaging supported by the French National Research Agency (ANR-10-INBS-04).

Funding

This work was supported by the European Union's Horizon 2020 research and innovation program under the Marie Sklodowska-Curie grant agreement 844070 to ABM, Défis scientifiques de l'Université Rennes 1 (17CQ436-S0) to ABM and GM, Ligue Régionale Contre le Cancer (22, 29, 35, 41, 72, 85) and the Fondation maladies rares (169608) to GM. GM laboratory also received institutional funding from the CNRS and the Université de Rennes 1.

Authors contribution

Conceptualization: A.B.M., G.M.; Methodology: A.B.M., F.D., O.N., A.P., G.M.; Validation: A.B.M., F.D., O.N., A.P., G.M.; Formal analysis: A.B.M., F.D., O.N., A.P., G.M.; Investigation: A.B.M., F.D., O.N., A.P., G.M.; Data curation: A.B.M., F.D., O.N., A.P., G.M.;

Writing - original draft: A.B.M.; Writing - review & editing: A.B.M., F.D., O.N., A.P., G.M.; Visualization: A.B.M., F.D., O.N., A.P, G.M.; Supervision: G.M.; Project administration: G.M.; Funding acquisition: A.B.M., G.M.

Conflict of interest

The authors declare no conflict of interest.

References

ACHILLEOS, A., WEHMAN, A. M. & NANCE, J. 2010. PAR-3 mediates the initial clustering and apical localization of junction and polarity proteins during C. elegans intestinal epithelial cell polarization. *Development,* 137**,** 1833-42.

ASAN, A., RAIDERS, S. A. & PRIESS, J. R. 2016. Morphogenesis of the C. elegans Intestine Involves Axon Guidance Genes. *PLoS Genet,* 12**,** e1005950.

BENESH, A. E., NAMBIAR, R., MCCONNELL, R. E., MAO, S., TABB, D. L. & TYSKA, M. J. 2010. Differential localization and dynamics of class I myosins in the enterocyte microvillus. *Mol Biol Cell,* 21**,** 970-8.

BIDAUD-MEYNARD, A., NICOLLE, O., HECK, M., LE CUNFF, Y. & MICHAUX, G. 2019. A V0-ATPase-dependent apical trafficking pathway maintains the polarity of the intestinal absorptive membrane. *Development,* 146.

BOSSINGER, O., FUKUSHIGE, T., CLAEYS, M., BORGONIE, G. & MCGHEE, J. D. 2004. The apical disposition of the Caenorhabditis elegans intestinal terminal web is maintained by LET-413. *Dev Biol,* 268**,** 448-56.

BRENNER, S. 1974. The genetics of Caenorhabditis elegans. *Genetics,* 77**,** 71-94.

BROEKS, A., JANSSEN, H. W., CALAFAT, J. & PLASTERK, R. H. 1995. A P-glycoprotein protects Caenorhabditis elegans against natural toxins. *EMBO J,* 14**,** 1858-66.

CHANG, J., CHANCE, M. R., NICHOLAS, C., AHMED, N., GUILMEAU, S., FLANDEZ, M., WANG, D., BYUN, D. S., NASSER, S., ALBANESE, J. M., CORNER, G. A., HEERDT, B. G., WILSON, A. J., AUGENLICHT, L. H. & MARIADASON, J. M. 2008. Proteomic changes during intestinal cell maturation in vivo. *J Proteomics,* 71**,** 530-46.

CHEN, Z. Y., HASSON, T., ZHANG, D. S., SCHWENDER, B. J., DERFLER, B. H., MOOSEKER, M. S. & COREY, D. P. 2001. Myosin-VIIb, a novel unconventional myosin, is a constituent of microvilli in transporting epithelia. *Genomics,* 72**,** 285-96.

CHINOWSKY, C. R., PINETTE, J. A., MEENDERINK, L. M., LAU, K. S. & TYSKA, M. J. 2020. Nonmuscle myosin-2 contractility-dependent actin turnover limits the length of epithelial microvilli. *Mol Biol Cell,* 31**,** 2803-2815.

CRAWLEY, S. W., MOOSEKER, M. S. & TYSKA, M. J. 2014a. Shaping the intestinal brush border. *J Cell Biol,* 207**,** 441-51.

CRAWLEY, S. W., SHIFRIN, D. A., JR., GREGA-LARSON, N. E., MCCONNELL, R. E., BENESH, A. E., MAO, S., ZHENG, Y., ZHENG, Q. Y., NAM, K. T., MILLIS, B. A., KACHAR, B. & TYSKA, M. J. 2014b. Intestinal brush border assembly driven by protocadherin-based intermicrovillar adhesion. *Cell,* 157**,** 433-446.

CROCE, A., CASSATA, G., DISANZA, A., GAGLIANI, M. C., TACCHETTI, C., MALABARBA, M. G., CARLIER, M. F., SCITA, G., BAUMEISTER, R. & DI FIORE, P. P. 2004. A novel actin barbed-end-capping activity in EPS-8 regulates apical morphogenesis in intestinal cells of Caenorhabditis elegans. *Nat Cell Biol,* 6**,** 1173-9.

DING, W. Y., ONG, H. T., HARA, Y., WONGSANTICHON, J., TOYAMA, Y., ROBINSON, R. C., NEDELEC, F. & ZAIDEL-BAR, R. 2017. Plastin increases cortical connectivity to facilitate robust polarization and timely cytokinesis. *J Cell Biol,* 216**,** 1371-1386.

EL MOURIDI, S., LECROISEY, C., TARDY, P., MERCIER, M., LECLERCQ-BLONDEL, A., ZARIOHI, N. & BOULIN, T. 2017. Reliable CRISPR/Cas9 Genome Engineering in Caenorhabditis elegans Using a Single Efficient sgRNA and an Easily Recognizable Phenotype. *G3 (Bethesda),* 7**,** 1429-1437.

FAUST, J. J., MILLIS, B. A. & TYSKA, M. J. 2019. Profilin-Mediated Actin Allocation Regulates the Growth of Epithelial Microvilli. *Curr Biol,* 29**,** 3457-3465 e3.

FELDMAN, J. L. & PRIESS, J. R. 2012. A role for the centrosome and PAR-3 in the hand-off of MTOC function during epithelial polarization. *Curr Biol,* 22**,** 575-82.

GAETA, I. M., MEENDERINK, L. M., POSTEMA, M. M., CENCER, C. S. & TYSKA, M. J. 2021. Direct visualization of epithelial microvilli biogenesis. *Curr Biol*.

GALLY, C., WISSLER, F., ZAHREDDINE, H., QUINTIN, S., LANDMANN, F. & LABOUESSE, M. 2009. Myosin II regulation during C. elegans embryonic elongation: LET-502/ROCK, MRCK-1 and PAK-1, three kinases with different roles. *Development,* 136**,** 3109-19.

GARBETT, D. & BRETSCHER, A. 2012. PDZ interactions regulate rapid turnover of the scaffolding protein EBP50 in microvilli. *J Cell Biol,* 198**,** 195-203.

GEISLER, F., COCH, R. A., RICHARDSON, C., GOLDBERG, M., BEVILACQUA, C., PREVEDEL, R. & LEUBE, R. E. 2020. Intestinal intermediate filament polypeptides in C. elegans: Common and isotype-specific contributions to intestinal ultrastructure and function. *Sci Rep,* 10**,** 3142.

GEISLER, F., COCH, R. A., RICHARDSON, C., GOLDBERG, M., DENECKE, B., BOSSINGER, O. & LEUBE, R. E. 2019. The intestinal intermediate filament network responds to and protects against microbial insults and toxins. *Development,* 146.

GOBEL, V., BARRETT, P. L., HALL, D. H. & FLEMING, J. T. 2004. Lumen morphogenesis in C. elegans requires the membrane-cytoskeleton linker erm-1. *Dev Cell,* 6**,** 865-73.

GORELIK, J., SHEVCHUK, A. I., FROLENKOV, G. I., DIAKONOV, I. A., LAB, M. J., KROS, C. J., RICHARDSON, G. P., VODYANOY, I., EDWARDS, C. R., KLENERMAN, D. & KORCHEV, Y. E. 2003. Dynamic assembly of surface structures in living cells. *Proc Natl Acad Sci U S A,* 100**,** 5819-22.

GRIMM-GUNTER, E. M., REVENU, C., RAMOS, S., HURBAIN, I., SMYTH, N., FERRARY, E., LOUVARD, D., ROBINE, S. & RIVERO, F. 2009. Plastin 1 binds to keratin and is required for terminal web assembly in the intestinal epithelium. *Mol Biol Cell,* 20**,** 2549-62.

HEINTZELMAN, M. B., HASSON, T. & MOOSEKER, M. S. 1994. Multiple unconventional myosin domains of the intestinal brush border cytoskeleton. *J Cell Sci,* 107 (Pt 12)**,** 3535-43.

HOUDUSSE, A. & TITUS, M. A. 2021. The many roles of myosins in filopodia, microvilli and stereocilia. *Curr Biol,* 31**,** R586-R602.

HUNT-NEWBURY, R., VIVEIROS, R., JOHNSEN, R., MAH, A., ANASTAS, D., FANG, L., HALFNIGHT, E., LEE, D., LIN, J., LORCH, A., MCKAY, S., OKADA, H. M., PAN, J., SCHULZ, A. K., TU, D., WONG, K., ZHAO, Z., ALEXEYENKO, A., BURGLIN, T., SONNHAMMER, E., SCHNABEL, R., JONES, S. J., MARRA, M. A., BAILLIE, D. L. & MOERMAN, D. G. 2007. High-throughput in vivo analysis of gene expression in Caenorhabditis elegans. *PLoS Biol,* 5**,** e237.

KHAN, L. A., JAFARI, G., ZHANG, N., MEMBRENO, E., YAN, S., ZHANG, H. & GOBEL, V. 2019. A tensile trilayered cytoskeletal endotube drives capillary-like lumenogenesis. *J Cell Biol,* 218**,** 2403-2424.

KOLOTUEV, I., SCHWAB, Y. & LABOUESSE, M. 2009. A precise and rapid mapping protocol for correlative light and electron microscopy of small invertebrate organisms. *Biol Cell,* 102**,** 121-32.

LAUWAET, T., OLIVEIRA, M. J., CALLEWAERT, B., DE BRUYNE, G., MAREEL, M. & LEROY, A. 2004. Proteinase inhibitors TPCK and TLCK prevent Entamoeba histolytica induced disturbance of tight junctions and microvilli in enteric cell layers in vitro. *Int J Parasitol,* 34**,** 785-94.

LEUNG, B., HERMANN, G. J. & PRIESS, J. R. 1999. Organogenesis of the Caenorhabditis elegans intestine. *Dev Biol,* 216**,** 114-34.

LIANG, J., SHAULOV, Y., SAVAGE-DUNN, C., BOISSINOT, S. & HOQUE, T. 2017. Chloride intracellular channel proteins respond to heat stress in Caenorhabditis elegans. *PLoS One,* 12**,** e0184308.

MACQUEEN, A. J., BAGGETT, J. J., PERUMOV, N., BAUER, R. A., JANUSZEWSKI, T., SCHRIEFER, L. & WADDLE, J. A. 2005. ACT-5 is an essential Caenorhabditis elegans actin required for intestinal microvilli formation. *Mol Biol Cell,* 16**,** 3247-59.

MANGEAT, T., LABOUESSE, S., ALLAIN, M., NEGASH, A., MARTIN, E., GUÉNOLÉ, A., POINCLOUX, R., ESTIBAL, C., BOUISSOU, A., CANTALOUBE, S., VEGA, E., LI, T., TROUVIÈRE, C., ALLART, S., KELLER, D., DEBARNOT, V., WANG, X. B., MICHAUX, G., PINOT, M., LE BORGNE, R., TOURNIER, S., SUZANNE, M., IDIER, J. & SENTENAC, A. 2021. Super-resolved live-cell imaging using random illumination microscopy. *Cell Reports Methods,* 1.

MARIADASON, J. M., NICHOLAS, C., L'ITALIEN, K. E., ZHUANG, M., SMARTT, H. J., HEERDT, B. G., YANG, W., CORNER, G. A., WILSON, A. J., KLAMPFER, L., ARANGO, D. & AUGENLICHT, L. H. 2005. Gene expression profiling of intestinal epithelial cell maturation along the crypt-villus axis. *Gastroenterology,* 128**,** 1081-8.

MCGHEE, J. D. 2007. The C. elegans intestine. *WormBook***,** 1-36.

MEENDERINK, L. M., GAETA, I. M., POSTEMA, M. M., CENCER, C. S., CHINOWSKY, C. R., KRYSTOFIAK, E. S., MILLIS, B. A. & TYSKA, M. J. 2019. Actin Dynamics Drive Microvillar Motility and Clustering during Brush Border Assembly. *Dev Cell,* 50**,** 545-556 e4.

NICOLLE, O., BUREL, A., GRIFFITHS, G., MICHAUX, G. & KOLOTUEV, I. 2015. Adaptation of Cryo-Sectioning for IEM Labeling of Asymmetric Samples: A Study Using Caenorhabditis elegans. *Traffic,* 16**,** 893-905.

POSTEMA, M. M., GREGA-LARSON, N. E., NEININGER, A. C. & TYSKA, M. J. 2018. IRTKS (BAIAP2L1) Elongates Epithelial Microvilli Using EPS8-Dependent and Independent Mechanisms. *Curr Biol,* 28**,** 2876-2888 e4.

RAMALHO, J. J., SEPERS, J. J., NICOLLE, O., SCHMIDT, R., CRAVO, J., MICHAUX, G. & BOXEM, M. 2020. C-terminal phosphorylation modulates ERM-1 localization and dynamics to control cortical actin organization and support lumen formation during Caenorhabditis elegans development. *Development,* 147.

REMMELZWAAL, S., GEISLER, F., STUCCHI, R., VAN DER HORST, S., PASOLLI, M., KROLL, J. R., JAROSINSKA, O. D., AKHMANOVA, A., RICHARDSON, C. A., ALTELAAR, M., LEUBE, R. E., RAMALHO, J. J. & BOXEM, M. 2021. BBLN-1 is essential for intermediate filament organization and apical membrane morphology. *Curr Biol*.

SALLEE, M. D., PICKETT, M. A. & FELDMAN, J. L. 2021. Apical PAR complex proteins protect against epithelial assaults to create a continuous and functional intestinal lumen. *BioRxiv,* https://doi.org/10.1101/2020.10.28.359299.

SATO, K., NORRIS, A., SATO, M. & GRANT, B. D. 2014. C. elegans as a model for membrane traffic. *WormBook***,** 1-47.

SAUVANET, C., WAYT, J., PELASEYED, T. & BRETSCHER, A. 2015. Structure, regulation, and functional diversity of microvilli on the apical domain of epithelial cells. *Annu Rev Cell Dev Biol,* 31**,** 593-621.

SCOTT, K. G., YU, L. C. & BURET, A. G. 2004. Role of CD8+ and CD4+ T lymphocytes in jejunal mucosal injury during murine giardiasis. *Infect Immun,* 72**,** 3536-42.

SHAFAQ-ZADAH, M., BROCARD, L., SOLARI, F. & MICHAUX, G. 2012. AP-1 is required for the maintenance of apico-basal polarity in the C. elegans intestine. *Development,* 139**,** 2061-70.

SHANER, N. C., LAMBERT, G. G., CHAMMAS, A., NI, Y., CRANFILL, P. J., BAIRD, M. A., SELL, B. R., ALLEN, J. R., DAY, R. N., ISRAELSSON, M., DAVIDSON, M. W. & WANG, J. 2013. A bright monomeric green fluorescent protein derived from Branchiostoma lanceolatum. *Nat Methods,* 10**,** 407-9.

TYE-DIN, J. & ANDERSON, R. 2008. Immunopathogenesis of celiac disease. *Curr Gastroenterol Rep,* 10**,** 458-65.

VAN FURDEN, D., JOHNSON, K., SEGBERT, C. & BOSSINGER, O. 2004. The C. elegans ezrin-radixin-moesin protein ERM-1 is necessary for apical junction remodelling and tubulogenesis in the intestine. *Dev Biol,* 272**,** 262-76.

VANDUSSEN, K. L., STOJMIROVIC, A., LI, K., LIU, T. C., KIMES, P. K., MUEGGE, B. D., SIMPSON, K. F., CIORBA, M. A., PERRIGOUE, J. G., FRIEDMAN, J. R., TOWNE, J. E., HEAD, R. D. & STAPPENBECK, T. S. 2018. Abnormal Small Intestinal Epithelial Microvilli in Patients With Crohn's Disease. *Gastroenterology,* 155**,** 815-828.

VOGEL, G. F., KLEE, K. M., JANECKE, A. R., MULLER, T., HESS, M. W. & HUBER, L. A. 2015. Cargo-selective apical exocytosis in epithelial cells is conducted by Myo5B, Slp4a, Vamp7, and Syntaxin 3. *J Cell Biol,* 211**,** 587-604.

WAHARTE, F., BROWN, C. M., COSCOY, S., COUDRIER, E. & AMBLARD, F. 2005. A two-photon FRAP analysis of the cytoskeleton dynamics in the microvilli of intestinal cells. *Biophys J,* 88**,** 1467-78.

WALTON, K. D., FREDDO, A. M., WANG, S. & GUMUCIO, D. L. 2016. Generation of intestinal surface: an absorbing tale. *Development,* 143**,** 2261-72.

ZHANG, H., KIM, A., ABRAHAM, N., KHAN, L. A. & GOBEL, V. 2013. Vesicular sorting controls the polarity of expanding membranes in the C. elegans intestine. *Worm,* 2**,** e23702.

ZHANG, R. & HOU, A. 2013. Host-Microbe Interactions in Caenorhabditis elegans. *ISRN Microbiol,* 2013**,** 356451.

ZHOU, X., MASSOL, R. H., NAKAMURA, F., CHEN, X., GEWURZ, B. E., DAVIS, B. M., LENCER, W. I. & WALDOR, M. K. 2014. Remodeling of the intestinal brush border underlies adhesion and virulence of an enteric pathogen. *mBio,* 5.

Figure legends

Figure 1. TEM analysis of the brush border.

(A) Representative TEM images of the intestinal lumen at the *C. elegans* developmental stages indicated.

(B-E) Quantification of the lumen perimeter (B) and microvilli density (C), length (D), and width (E) from TEM images. Histograms show the mean ± SEM of the average of 3-13 slices (B), 3-10 lumen (C) and 6-29 microvilli (D-E) from 3-5 embryos. See Fig. S1 for detailed measurements of each embryo. Open arrows, nascent microvilli; filled arrows, empty spaces between microvilli; YA, young adults. n.s., non-significant, * p<0,05, **p<0,01, ***p<0,001, unpaired t-test.

(F) Transversal view of the brush border in adult worms.

(G) The distance between microvilli edges and centres was calculated on 200 microvilli from (F).

Figure 2. Brush border components are dynamically enriched at the apical membrane during microvilli assembly.

(A-I) Representative images of the apical expression of GFP-tagged MLC-5, PLST-1 and ACT-5, mNG-tagged ERM-1, IFB-2 and HUM-5, and mVenus-tagged FLN-2 in L1 larvae (A-D) and 1,5-fold embryos (E-I).

(J-K) The absolute apical signal of the indicated markers was measured using photon-counting detectors (see methods) on at least 10 embryos at the indicated developmental stages and normalized to the maximum expression for each marker. Data are mean ± SEM. (J) shows a focus on early brush border assembly steps where the maximum intensity was set at the 2-fold-stage.

(L-S) Apical localization of the indicated markers at the 2-fold stage.

In all images, arrowheads show the apical plasma membrane of the intestinal cells.

Figure 3. Super-resolution imaging of the brush border.

(A-B) Super-resolution images of ERM-1 endogenously tagged with BFP, mNG and wSc in *C. elegans* young adults. (B) represents the normalized intensity profile along a 4 µm-long dashed line, as represented in (A).

(C) Super-resolution images of ERM-1::mNG or EXL-1::mNG using a Zeiss LSM880-Airyscan or Random Illumination Microscopy.

(D) Transversal super-resolution image of the brush border performed on a *C. elegans* strain endogenously expressing ERM-1::mNG. The red hexagon indicates the putative hexagonal packing of microvilli.

(E-I) Super-resolution imaging of the indicated microvilli markers endogenously tagged with mNG (ERM-1, HUM-5,), GFP (PLST-1, MLC-5), BFP (EPS-8), mVenus (FLN-2) or wSc (IFB-2). Insert, higher magnification of the zone where ERM-1 and PLST-1 colocalize. Arrowheads show the microvilli base.

(J-K) Super-resolution images of the brush border in 2-fold embryo and L2 larvae co-expressing EPS-8::BFP, ERM-1::mNG and IFB-2::wSc. Left TEM images show the shape of the brush border at the corresponding developmental stage. Right histograms correspond to the signal intensity profile of the three markers along the line depicted on the pictures.

All the pictures were performed in young adult worms. Unless mentioned, scale bars are 2µm.

Figure 4. Brush border components dynamics during microvilli assembly.

(A-B) ERM-1::mNG was bleached in a 1,5-fold embryo and an adult worm, and fluorescence recovery was observed every 30 s.

(B-E) Quantification of the signal recovery after bleaching of ERM-1::mNG (B), EPS-8::mNG (C), ACT-5::GFP (D) and IFB-2::mNG (E), measured every 30 s on 5-11 worms at the indicated developmental stages. Thin lines represent the mean ± SEM of signal recovery. Bold lines represent one-phase association non-linear regression fitting curves.

(F-G) The mobile fraction of the indicated markers at the Comma, 1,5-fold, L1 larva and adult stages was calculated from the FRAP data from (B-E). Histogram show the mean ± SEM. The difference between variance was calculated using ANOVA, *p<0,05, **p<0,01.

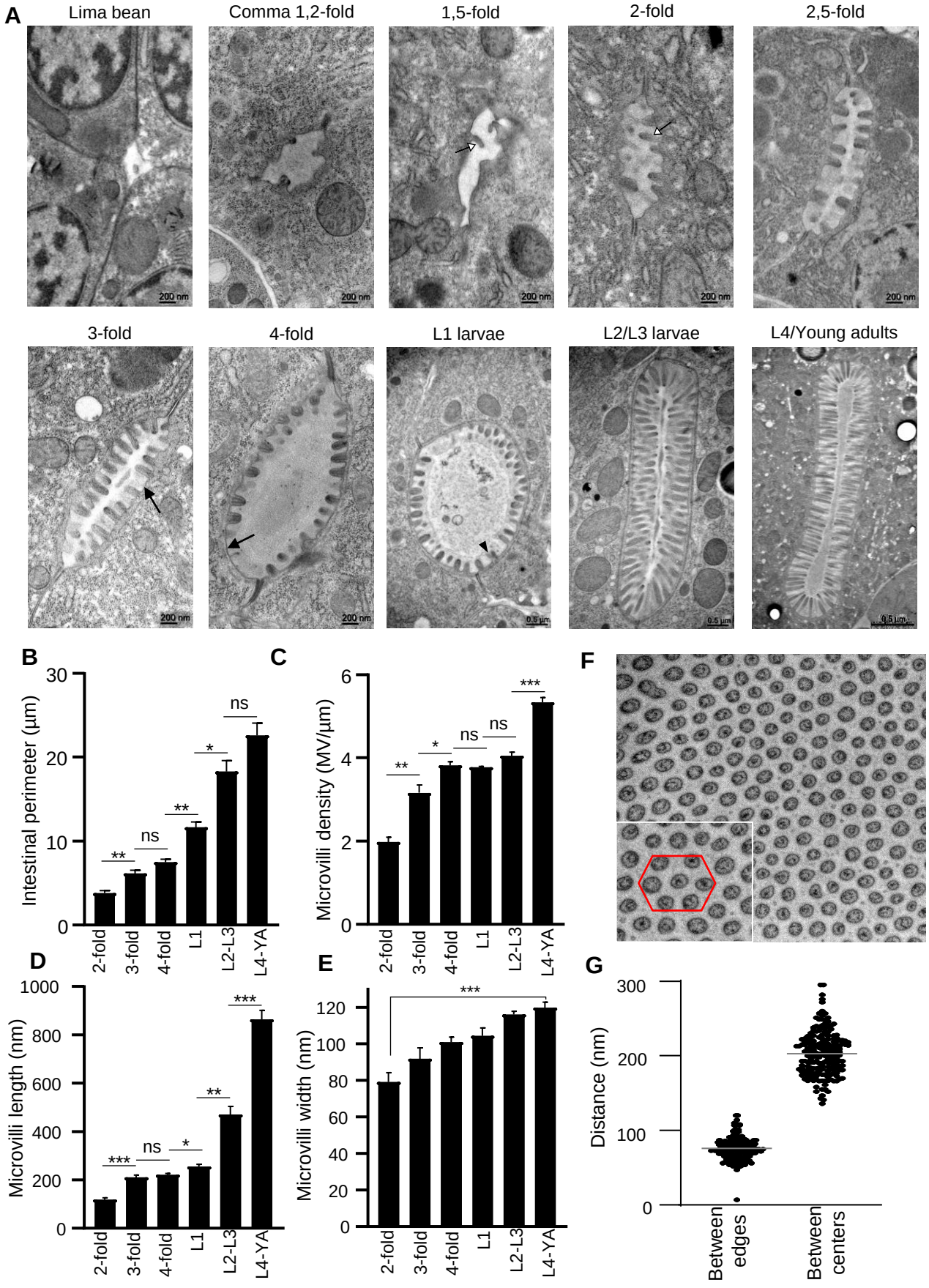
A
Lima bean
Comma 1,2-fold
1,5-fold
2-fold
2,5-fold
3-fold
4-fold
L1 larvae
L2/L3 larvae
L4/Young adults
200 nm
0.5 µm
B
Intestinal perimeter (µm)
C
Microvilli density (MV/µm)
D
Microvilli length (nm)
E
Microvilli width (nm)
F
G
Distance (nm)
Between edges
Between centers
2-fold
3-fold
4-fold
L1
L2-L3
L4-YA
ns
*
**
***

Figure 1

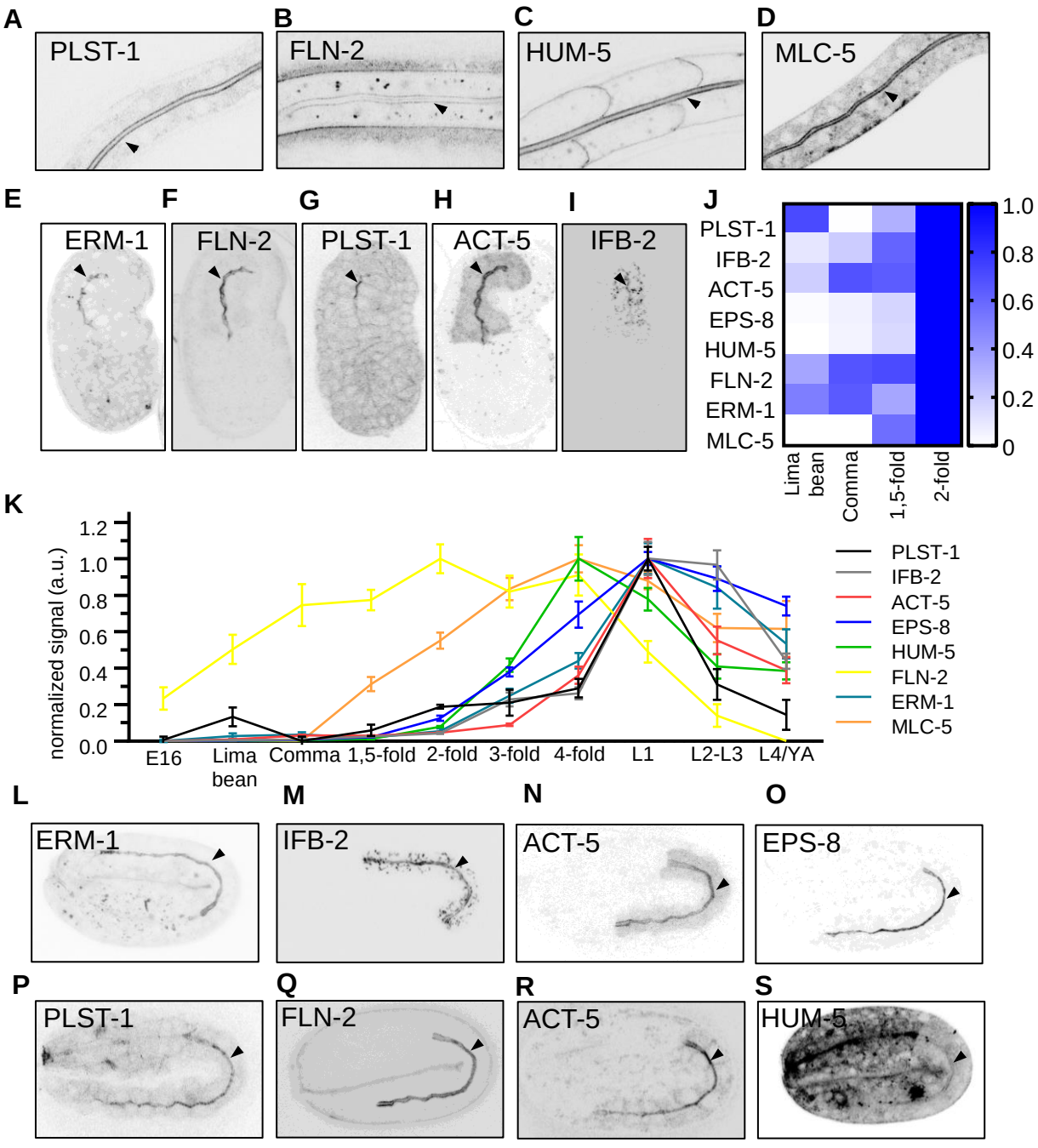
A
PLST-1
B
FLN-2
C
HUM-5
D
MLC-5
E
ERM-1
F
FLN-2
G
PLST-1
H
ACT-5
I
IFB-2
J
PLST-1
IFB-2
ACT-5
EPS-8
HUM-5
FLN-2
ERM-1
MLC-5
Lima bean
Comma
1,5-fold
2-fold
1.0
0.8
0.6
0.4
0.2
0
K
normalized signal (a.u.)
1.2
1.0
0.8
0.6
0.4
0.2
0.0
E16
Lima bean
Comma
1,5-fold
2-fold
3-fold
4-fold
L1
L2-L3
L4/YA
PLST-1
IFB-2
ACT-5
EPS-8
HUM-5
FLN-2
ERM-1
MLC-5
L
ERM-1
M
IFB-2
N
ACT-5
O
EPS-8
P
PLST-1
Q
FLN-2
R
ACT-5
S
HUM-5

Figure 2

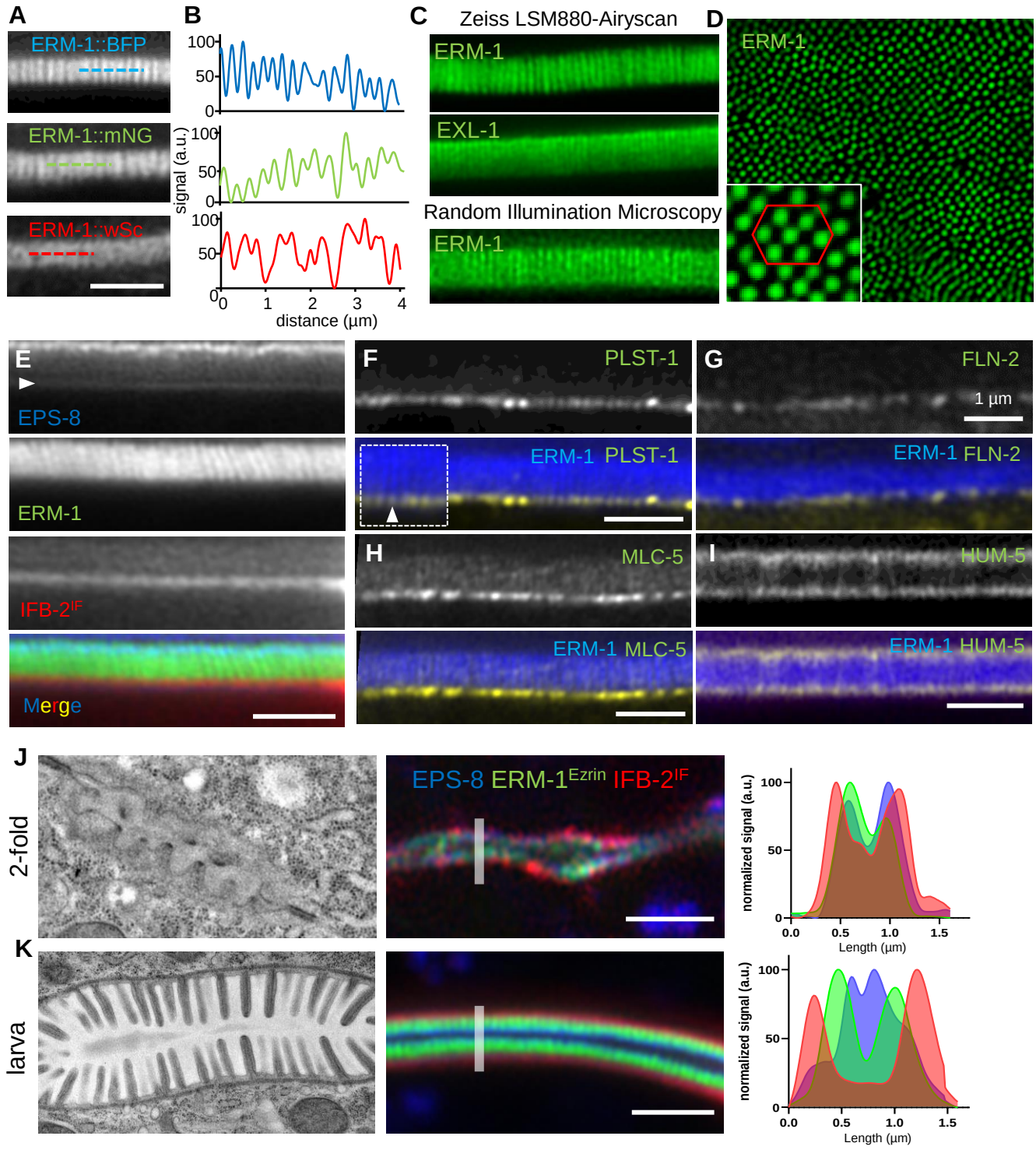
A
ERM-1::BFP
ERM-1::mNG
ERM-1::wSc
B
signal (a.u.)
distance (µm)
C
Zeiss LSM880-Airyscan
ERM-1
EXL-1
Random Illumination Microscopy
ERM-1
D
ERM-1
E
EPS-8
ERM-1
IFB-2IF
Merge
F
PLST-1
ERM-1 PLST-1
G
FLN-2
1 µm
ERM-1 FLN-2
H
MLC-5
ERM-1 MLC-5
I
HUM-5
ERM-1 HUM-5
J
2-fold
EPS-8 ERM-1Ezrin IFB-2IF
normalized signal (a.u.)
Length (µm)
K
larva
normalized signal (a.u.)
Length (µm)

Figure 3

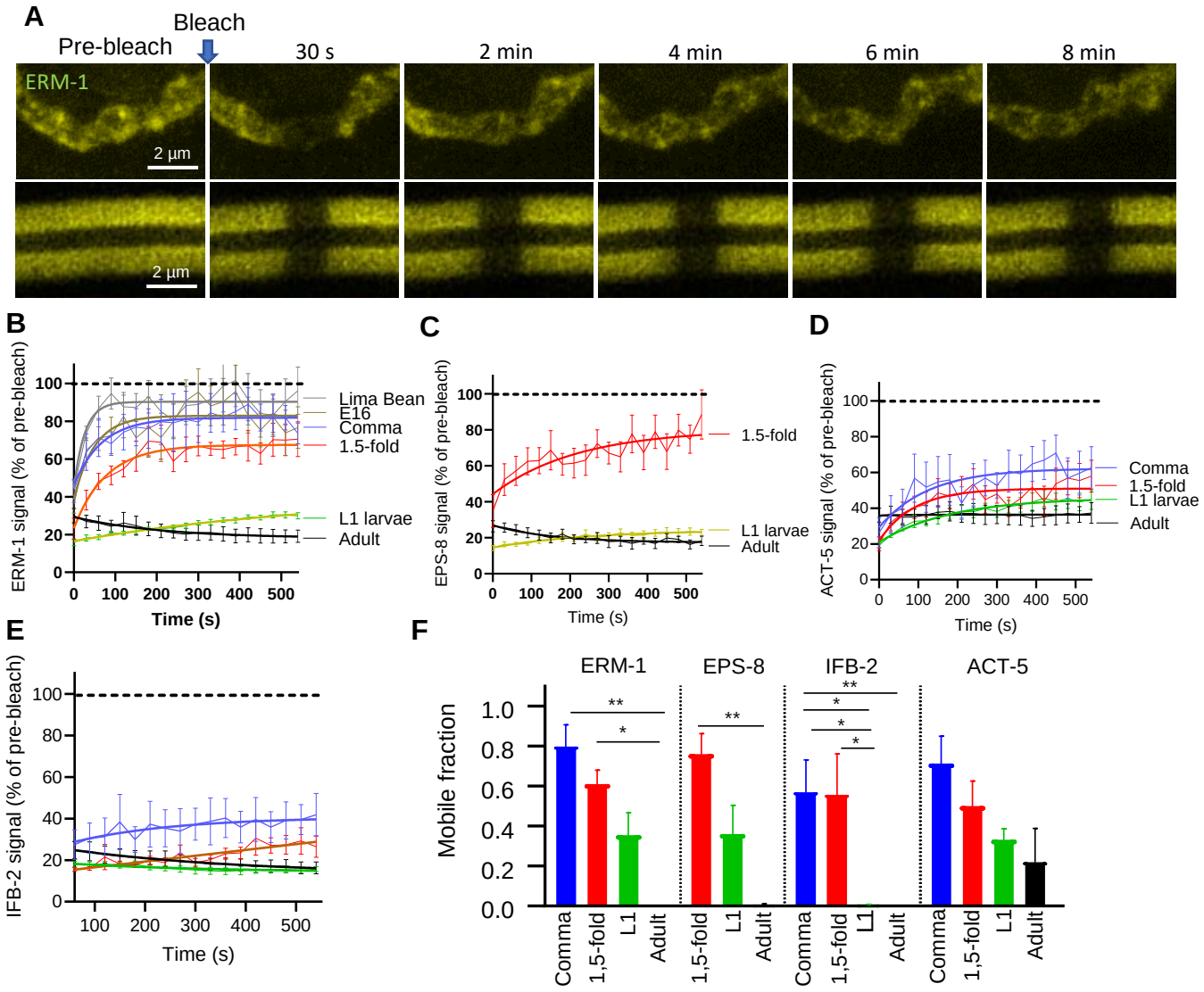
A
Pre-bleach
Bleach
30 s
2 min
4 min
6 min
8 min
ERM-1
2 µm
2 µm
B
ERM-1 signal (% of pre-bleach)
Time (s)
Lima Bean
E16
Comma
1.5-fold
L1 larvae
Adult
C
EPS-8 signal (% of pre-bleach)
Time (s)
1.5-fold
L1 larvae
Adult
D
ACT-5 signal (% of pre-bleach)
Time (s)
Comma
1.5-fold
L1 larvae
Adult
E
IFB-2 signal (% of pre-bleach)
Time (s)
F
Mobile fraction
ERM-1
EPS-8
IFB-2
ACT-5
Comma
1,5-fold
L1
Adult

Figure 4

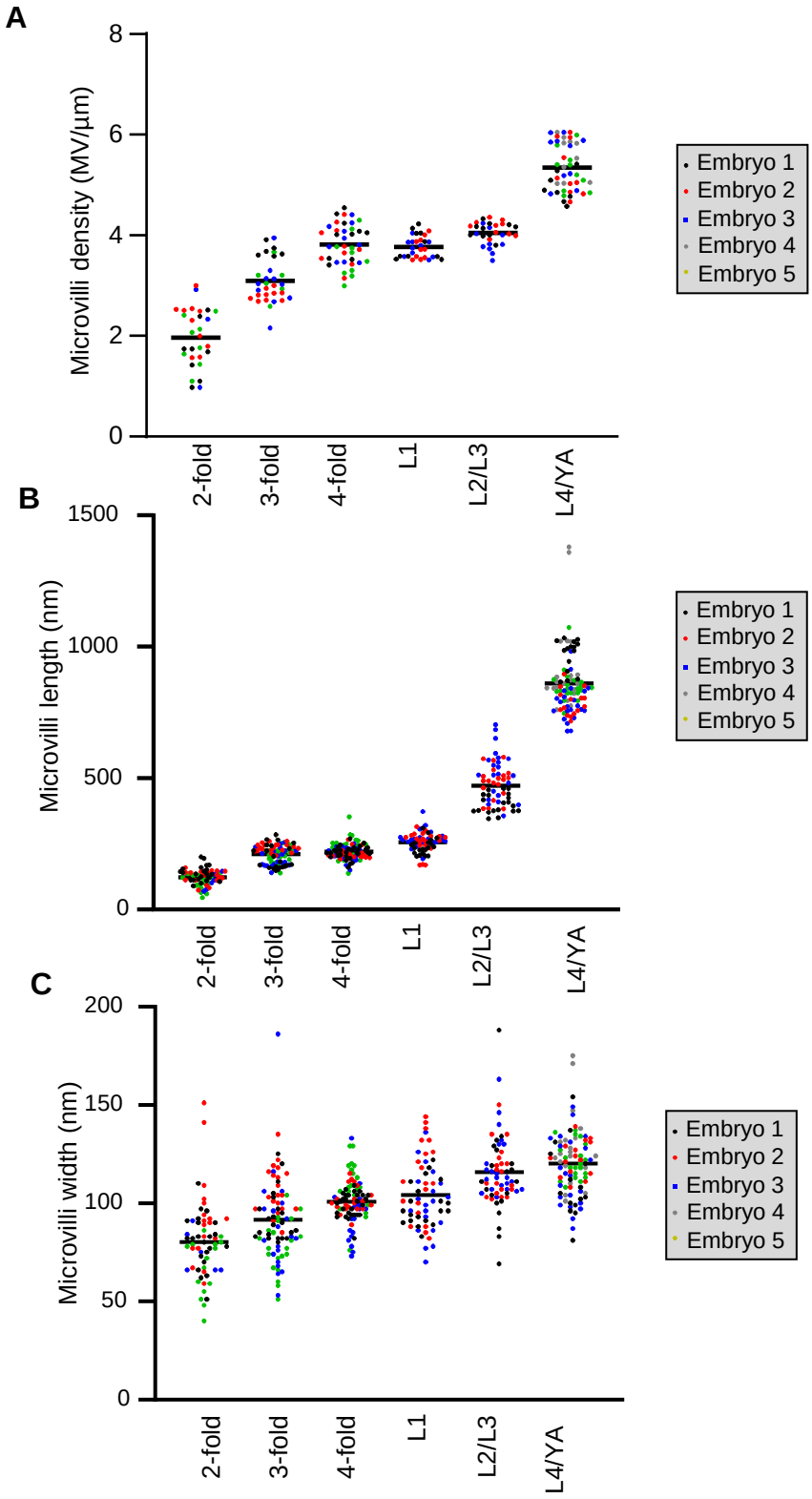

Figure S1. Individual values of brush border measurements by TEM.
Colorized dots represent individual worms at the indicated developmental stages. Bar is the grand mean of all the measurements. Microvilli density was measured on 3-13 slices/worm, microvilli length and width on 6-29 microvilli/worm.

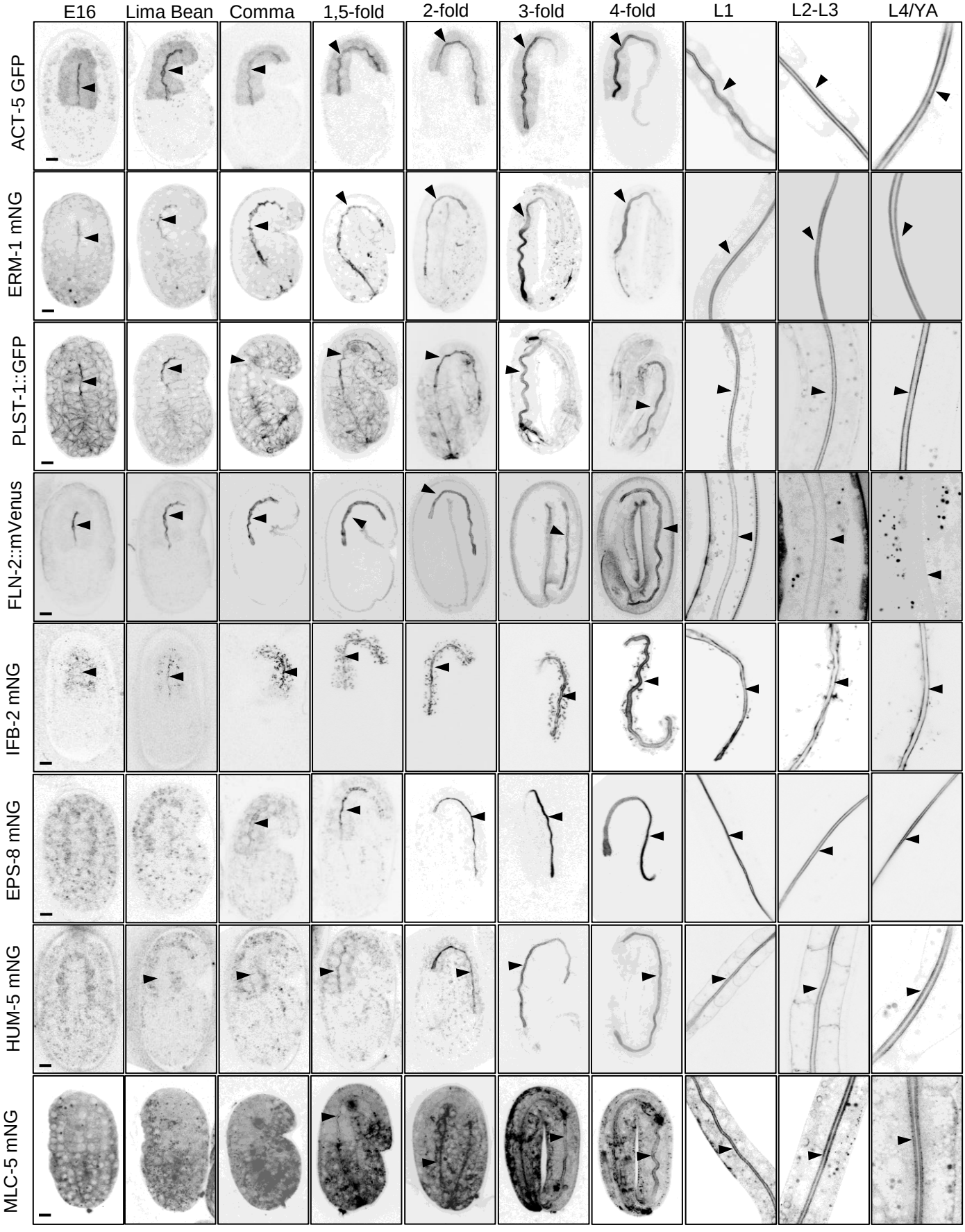

Figure S2. Systematic analysis of brush border markers during *C. elegans* development. Representative confocal images of the endogenously tagged markers indicated (except ACT-5::GFP). Arrowheads show the intestinal cells apical PM. Scale bar is 5 µm.

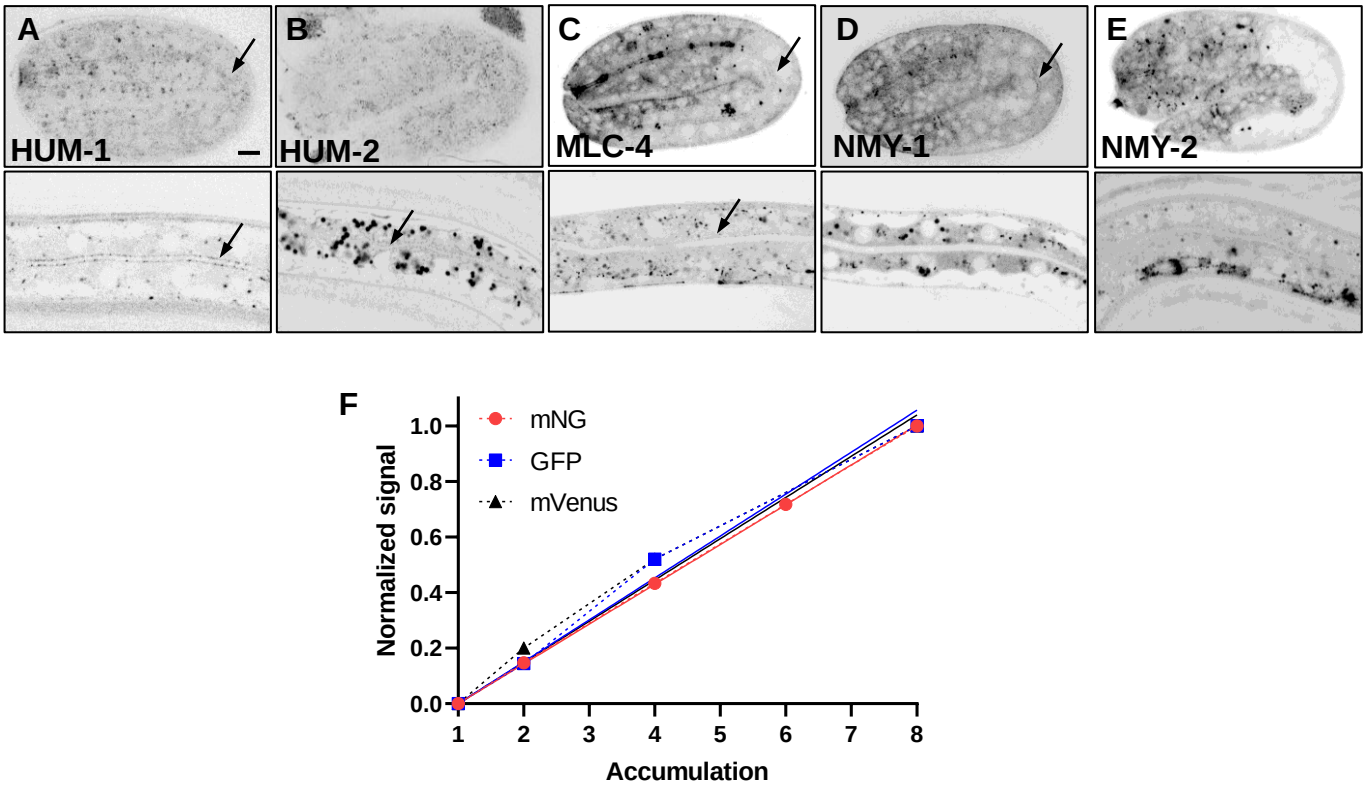

Figure S3. Systematic analysis of brush border markers during *C. elegans* development.
(A-E) Representative confocal images of *C. elegans* strains expressing endogenously tagged versions of the indicated markers, which showed no apical accumulation during *C. elegans* intestine development. (F) Control of the quantitative assessment of brush border markers arrival at the apical PM. Accumulation of ERM-1::mNG, PLST-1::GFP and FLN-2::mVenus signal linearly increases with the image accumulation. Scale bar, 5 µm.

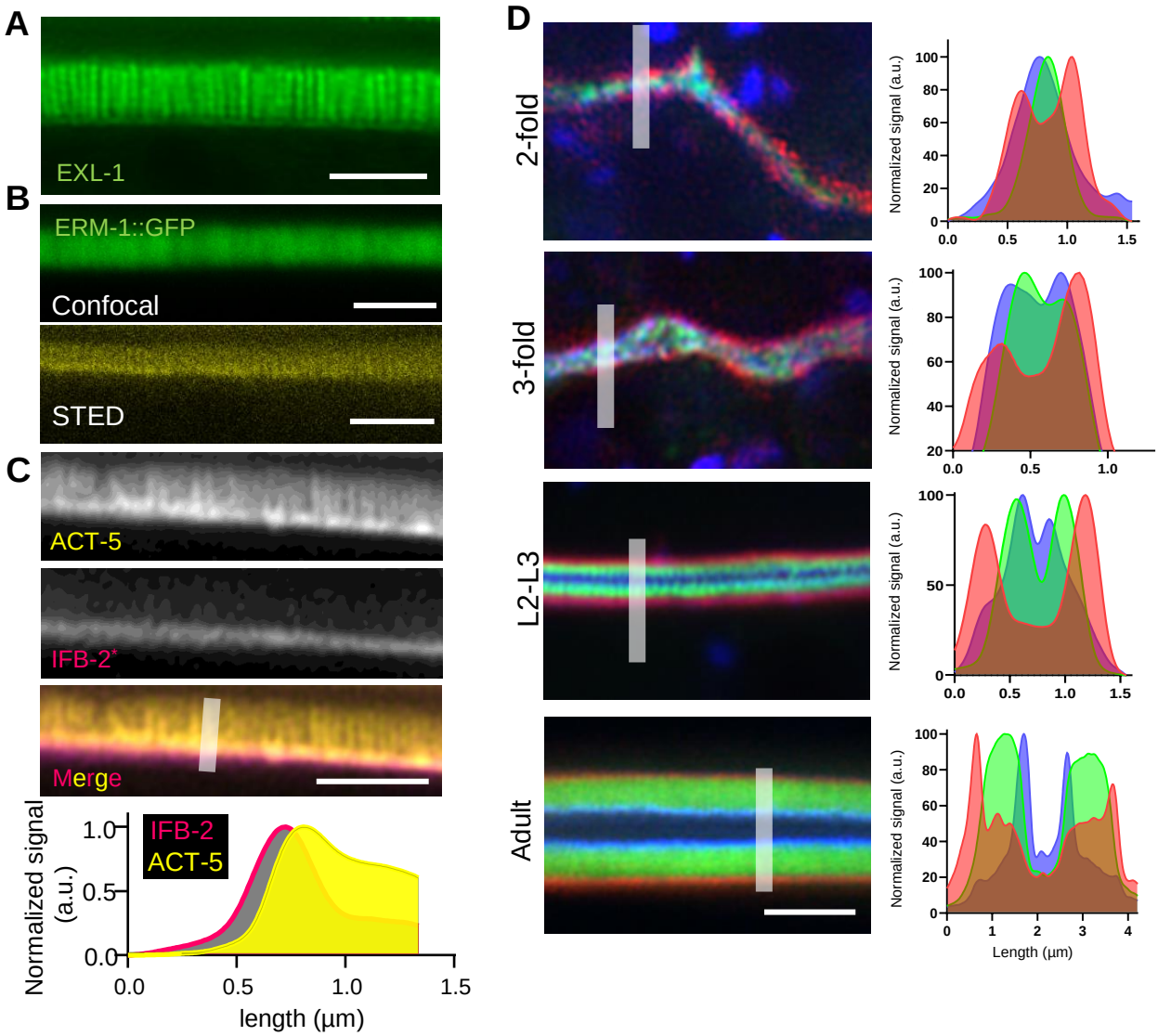

Figure S4. Super-resolution imaging of brush border markers *in vivo*. (A) Representative confocal image of exogenously expressed EXL-1::GFP. (B) ERM-1::GFP was imaged in adult worms using the indicated microscopes. (C) Super-resolution images of a *C. elegans* adults co-expressing ACT-5::GFP and IFB-2::wSc. Bottom panel shows a normalized intensity profile along the line depicted in grey. (D) Representative images of the localization of endogenously tagged EPS-8::BFP, ERM-1::mNG and IFB-2::wSc in *C. elegans* at the indicated developmental stages. Right panels show an intensity profile of the three markers along the line depicted in left panels. Scale bars, 2µm.

.

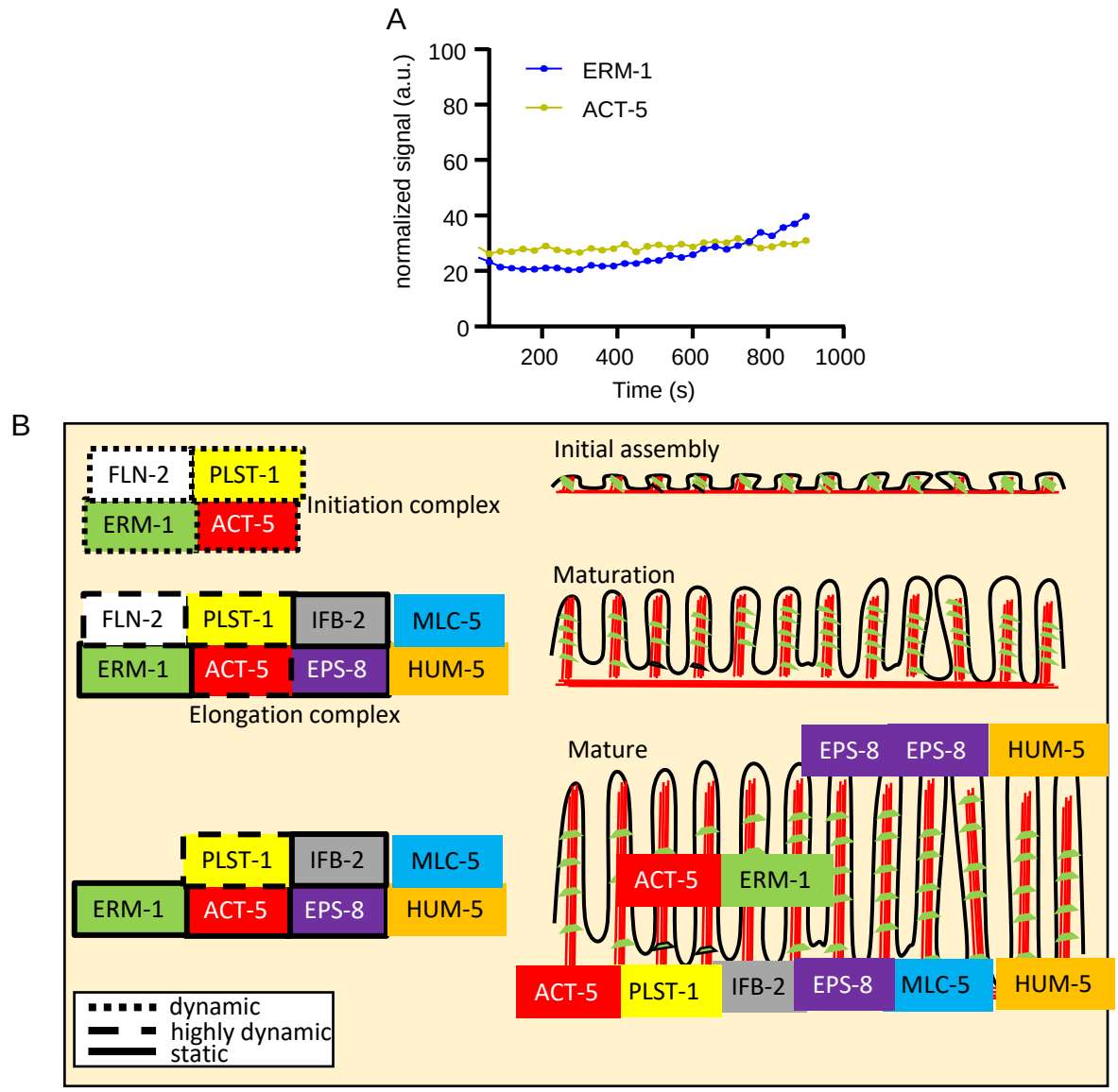

Figure S5. Dynamic recruitment of brush border components.
(A) Longer measurement of ERM-1 and ACT-5 dynamics in adult worms. The curves show the recovery of ERM-1::mNG and ACT-5::GFP signal every 30 s after photobleaching, measured for an extended time. (B) Model of brush border assembly *in vivo* in *C. elegans*. Microvilli are built from a preformed *initiation complex* and assemble through the dynamic recruitment of brush border components, which become highly stable in the mature brush border.

Strain	Markers	Genotype	Reference
FBR 96	MLC-4	mlc-4(jme04[mlc-4::eGFP+loxP])III	Francois Robin lab
FBR140	MLC-5	mlc-5(jme09[GFP^3xFLAG::mlc-5])III	Francois Robin lab
FBR222	FLN-2	fln-2::venus	Francois Robin lab
FL274	ERM-1, IFB-2	erm-1(bab59[erm-1::mNG^SEC^3xFlag]) I ; ifb-2(bab142[ifb-2::wSc]) II	Bidaud-Meynard et al., Development, 2019
FL290	EPS-8	eps-8(bab140[eps-8::mNG]) IV	This study
FL378	ERM-1	erm-1(bab59[erm-1::mNG^3xFlag]) I	Bidaud-Meynard et al., Development, 2019
FL379	ERM-1	bab64[erm-1::wrmSc^3xFlag] I	Bidaud-Meynard et al., Development, 2019
FL383	EPS-8, ERM-1, IFB-2	eps-8(bab140[eps-8::mNG]) IV ; erm-1(bab59[erm-1::mNG^SEC^3xFlag]) I; IFB-2	This study
FL384	ERM-1	erm-1(bab167[erm-1::degron-tagBFP2])	This study
FL385	IFB-2	ifb-2(bab153[ifb-2::mNG]) II	This study
FL386	ERM-1, PLST1	erm-1(bab167[erm-1::degron-tagBFP2]) ; plst-1(msn190[plst-1::gfp]) IV	This study
FL387	ERM1, HUM5	erm-1(bab167[erm-1::degron-tagBFP2]) ; hum-5(bab189[hum-5::mNG])	This study
FL388	ERM-1, MLC5	erm-1(bab167[erm-1::degron-tagBFP2]) ; mlc-5(jme09[GFP^3xFLAG::mlc-5])III	This study
FL586	ERM-1, FLN-2	erm-1(bab167[erm-1::degron-tagBFP2])	This study
LP162	NMY-2	nmy-2(cp13[nmy-2::GFP + LoxP]) I	CGC
LP462	MRCK-1	mrck-1(cp189[mrck-1::GFP::3xFlag]) V	CGC
MCP111	PGP-1	pgp-1(bab111[mNG^3xFlag::pgp-1]) IV	Bidaud-Meynard et al., Development, 2019
MCP184	HUM-2	hum-2(bab184[hum-2::mNG])	This study
MCP189	HUM-5	hum-5(bab189[hum-5::mNG])	This study
MCP223	EXL-1	exl-1(bab223[exl-1::mNG])	This study
ML2540	NMY-1	nmy-1(mc82[nmy-1::gfp]) X.	Vuong-Brender TTK, et al. eLife 2017
OH2211	EXL-1	otEx1184 [exl-1p::exl-1::GFP + rol-6(su1006)]	CGC
QQ226	HUM-1	hum-1(cv21[hum-1::RFP]) I	CGC
RZB213	PLST-1	plst-1 (msn190[plst-1::gfp]) IV	Ding WY et al J Cell Biol 2017
VJ268	ACT-5	fgEx12 (act-5p::act-5::gfp)	Zhang et al., 2012

Table S1. *C. elegans* strains used in this study.